Proceedings of ICFDP7 :
Seventh International Congress on Fluid Dynamics and Propulsion
December 18-20, 2001, Cairo, Egypt

ICFDP7-2001074

STUDY OF A TURBULENT CYLINDRICAL WALL JET IMPINGING NORMALLY ON A FLAT PLATE

A.T. M. Rofiqul Islam
Graduate School of Engineering
Gifu University, Japan

Yasuaki Kozato
Department of Mechanical and Systems
Engineering, Gifu University, Japan

Shigeki Imao
Department of Mechanical and Systems
Engineering, Gifu University, Japan

Toshio Tanaka
Department of Mechanical and Systems
Engineering, Gifu University, Japan

ABSTRACT

This is an experimental study of a turbulent cylindrical wall jet that issues from an annular nozzle, flows along a cylindrical wall and finally impinges normally on a flat plate. This type of jet flow has properties characterized by a pressure increase in the downstream direction, a boundary layer separation from the cylindrical wall, and a reattachment on the impingement plate. This report mainly concerns the effect of various nozzle-impingement distances on the jet properties in the region before and after the impingement. The mean and turbulent velocities and the Reynolds stress were measured with a constant-temperature hot-wire anemometer. Variations in the static pressure on the cylindrical wall., the maximum jet velocity, the half-width of the jet, and the boundary layer thickness in the downstream direction were examined. The flow field can be classified into three regions: a cylindrical wall jet region, an impingement region, and a radial wall jet region. The length of these regions is dependent on the nozzle-impingement distance.

Keywords: Cylindrical wall jet, Annular nozzle, Impingement, Separation, Reattachment, Radial wall jet

INTRODUCTION

Since jet flow is used in many industrial applications, numerous theoretical and experimental studies referred to the jet have been done[1-3] . Although many studies concerning an impinging jet flow on the body have been conducted, most of them are related to the normal impingement of a circular free jet on a flat plate[4-6].

When a cylindrical wall jet issuing from an annular nozzle, flowing along a cylindrical wall impinges normally on a flat plate, the boundary layer on the cylindrical wall grows, and pressure in the flow increases in the downstream direction, i.e., an adverse pressure gradient exists along the cylindrical wall. As a result, the flow separates from the cylindrical wall and later reattaches on the impingement plate. Consequently, the recirculating flow exists in the corner region between the cylindrical wall and the impingement plate. It should be considered that this flow has some characteristics different from the normal impinging circular free jet on the flat plate.

This paper presents an experimental study on a turbulent cylindrical wall jet impinging normally on a flat plate. The main objective of this study is to obtain the flow characteristics of an impinging cylindrical wall jet on a flat plate. The mean and turbulent velocity components, the Reynolds stress, the static pressure in the flow, and the wall static pressure were measured for various nozzle-impingement distances (distance between annular nozzle exit and impingement plate), and, the characteristics of the jet flow in the downstream direction were obtained.

The results show that the flow field can be classified into three regions: a cylindrical wall jet region, an impingement region, and a radial wall jet region. The effect of the nozzle-impingement distance on the flow pattern in the impingement region, and the separation point from the cylindrical wall and the reattachment point on the impingement plate were made clear. The results were compared with those of the cylindrical wall jet[7] and the impinging circular free jet on the flat plate.

NOMENCLATURE

The coordinate system and main notations are shown in Fig.1.

- b : half-width of jet (distance from cylindrical wall to point of $Um/2$ in lateral velocity distribution) , mm
- b_1 : half-width of radial wall jet after impingement, mm
- Cp : local static pressure coefficient = $(p - pa)/(1/2)\ \rho Uo^2$
- Cpc : wall pressure on cylindrical wall, dimensionless
- Cpm : maximum pressure on impingement plate, dimensionless
- Cps : stagnation pressure on impingement plate, dimensionless
- Cpw : wall pressure on impingement plate, dimensionless
- d : diameter of circular cylinder, mm
- D : diameter of circular nozzle, mm
- L : distance between annular nozzle exit and impingement plate, mm

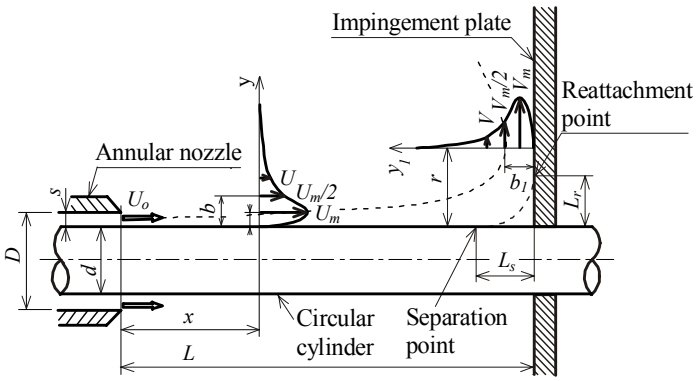

Fig.1 Coordinate system and main notations

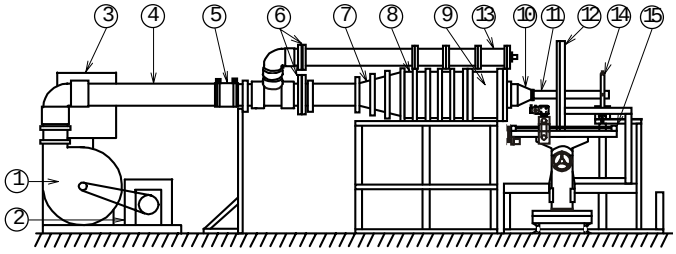

(1) Turbo blower
(2) Variable motor
(3) Air filter
(4) Circular duct
(5) Vibration damper
(6) Shutter
(7) Diffuser
(8) Settling chamber
(9) Plenum chamber
(10) Annular nozzle
(11) Circular cylinder
(12) Impingement plate
(13) Calibration nozzle
(14) End support of circular cylinder
(15) Automatic traversing device

Fig.2 Experimental apparatus

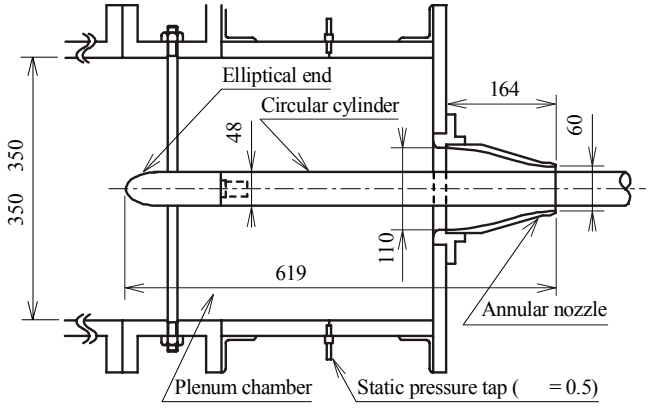

Fig.3 Plenum chamber, annular nozzle and circular cylinder

- Lr : distance from cylindrical wall to reattachment point on impingement plate, mm
- Ls : distance from impingement plate to separation point on cylindrical wall, mm
- p : local static pressure, Pa
- p_a : atmospheric pressure, Pa
- p_c : pressure on cylindrical wall, Pa
- p_m : maximum pressure on impingement plate, Pa
- p_s : stagnation pressure on impingement plate, Pa
- p_w : pressure on impingement plate, Pa
- r : radial distance measured from cylindrical wall along impingement plate, mm
- Re : Reynolds number at annular nozzle exit, dimensionless
- s : width of annular nozzle = $(D-d)/2$, mm
- u, v, w : fluctuating velocity components in x-, y- and z-directions, m/s
- u', v', w' : rms values of u, v and w, m/s
- U, V, W : time-mean velocity components in x-, y- and z-directions, m/s
- Uo : discharge velocity at annular nozzle exit, m/s
- Um : maximum value of U measured in y-direction, m/s
- Vm : maximum value of V measured in y_1-direction, m/s
- x : distance measured from nozzle exit along cylindrical wall, ,mm
- y : distance measured normal from x-axis, mm
- y_1 : distance measured normal from r-axis, mm
- δ : boundary layer thickness (distance from cylindrical wall to maximum jet velocity point), mm

EXPERIMENTAL APPARATUS AND PROCEDURE

Experimental Apparatus

Figure 2 illustrates the experimental apparatus used in this study. A turbo blower (1) with a flow rate of 0.75 m^3/s and static pressure of 3.4 kPa is driven by a 7.5 kW variable motor (2). Honeycombs with a cell size of 8 mm and length of 150 mm are installed in a circular duct (4). Screens with 30 and 40 meshes are arranged in a diffuser (7) and a settling chamber (8). A plenum chamber (9) with a 350 mm × 350 mm cross-section is made of a 20 mm thick acrylic plate. An annular nozzle (10) is attached to the downstream wall of the plenum chamber so that the jet issues from the nozzle and flows along the wall surface of a circular cylinder (11), impinging normally on an impingement plate (12). This plate is made of a 20 mm thick square acrylic plate (800 mm × 800 mm). A calibration nozzle (13) is used to calibrate the performance of the hot-wire probe.

Details of the plenum chamber, annular nozzle and circular cylinder are shown in Fig. 3. The contraction ratio of the annular nozzle exit to the plenum chamber is about 1:120. Since the diameter of the annular nozzle is 60 mm, the outside diameter of the circular cylinder is 48 mm, and the axis of the jet is aligned with the central axis of the circular cylinder, the gap between the annular nozzle and the circular cylinder (width of the annular nozzle), s, is 6 mm.

Experimental Method

The time-mean and fluctuating velocity components in the x-, y- and z-directions and the Reynolds stress were measured with a turnable I-type and a turnable inclined-type hot-wire probes. Furthermore, a tandem-type hot-wire probe was used to measure the mean velocity near the wall surface and to decide the directions of forward and reverse flow. These probes were calibrated in a uniform air flow before and after each test run. The output signals were

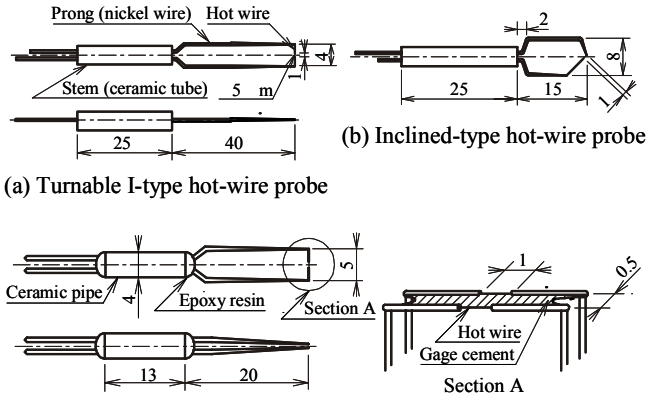

Table 1 Experimental conditions

Experimental description		Dimensions
Diameter of circular cylinder	d [mm]	48
Diameter of annular nozzle	D [mm]	60
Nozzle width	s [mm]	6
Nozzle exit velocity	U_0 [m/s]	40
Nozzle impingement distance	L/s	1 50
Reynolds number	Re	1.54×10^4

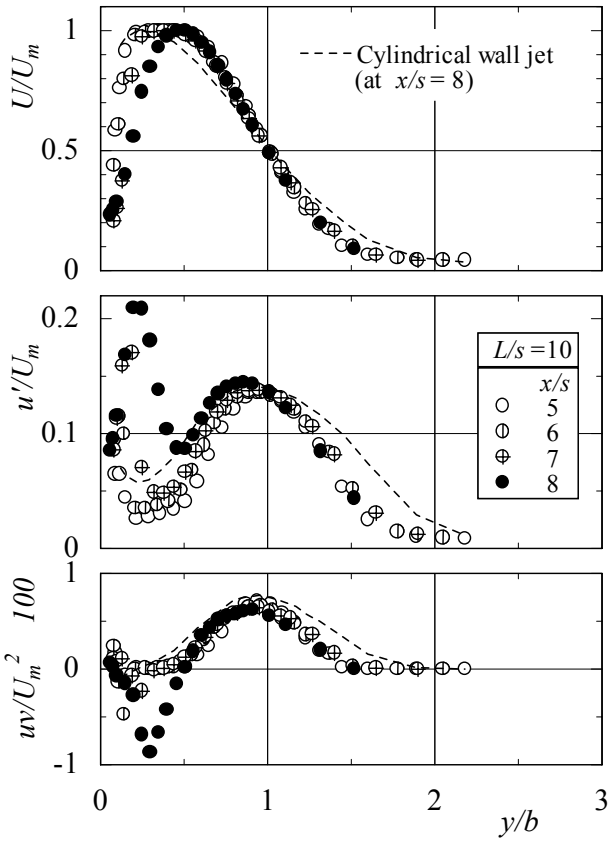

Fig.5 Mean velocity and turbulent intensity profiles in *x*-direction and Reynolds stress distribution

linearized by a constant-temperature hot-wire anemometer and saved on a hard-disk drive as time series data using an A-D converter (sampling frequency: 10 kHz; sampling time:12 sec). Using these data, each velocity component was calculated with a personal computer.

Figure 4 illustrates three types of hot-wire probe used in this study. The turnable I-type and turnable inclined-type hot-wire probes consist of a single tungsten wire with a sensor length and diameter of 1 mm and 5μm, respectively. The tandem-type hot-wire probe consists of two parallel tungsten wires with similar sensor configurations and wires separated by 4 mm. The space between the two parallel wires is filled with gage adhesive.

The static pressure distributions on the cylindrical wall surface and in the flow near the wall (y < 10 mm), and across the jet away from the wall (y > 10 mm) were measured using a half disk-type pressure probe and a disk-type pressure probe[8], respectively. All static pressures were measured with an analog electronic manometer via a pressure transducer.

The measurement uncertainty *Urss* is 3.0 % for the mean velocity. The measurement accuracy of the static pressure is about ± 0.1 Pa.

Experimental Conditions

The experiments were carried out under the conditions described in Table 1. During the experiments, all the measurements were taken at nozzle width, s = 6 mm, nozzle exit velocity, Uo = 40 m/s, and Reynolds number at the nozzle exit, $Re = Uos/\nu = 1.54\times10^4$.

The ratio of the distance between the annular nozzle exit and the impingement plate L to the annular nozzle width s, L/s (hereafter called the nozzle-impingement distance) was varied from 1 to 50.

EXPERIMENTAL RESULTS AND DISCUSSION

As preliminary experiments, the general properties of a circular free jet, and of a cylindrical wall jet were examined to check the elementary flow properties of the present study. Also, it is confirmed that the jet flow is axially symmetric from measuring the velocity profiles around the circular cylinder.

Mean Velocity and Turbulent Intensity Profiles

Mean velocities and turbulent intensities in the x-, y-, and z-directions at different sections are obtained for various nozzle-impingement distance L/s. Some results for the x-direction are mentioned in this report.

Figure 5 illustrates the mean velocity and turbulent intensity profiles in the x-direction at different sections x/s = 5, 6, 7, 8 for the nozzle-impingement distance, L/s = 10. The dotted lines in the figure represent the corresponding profiles of a cylindrical wall jet (without impingement) at the section of x/s = 8.

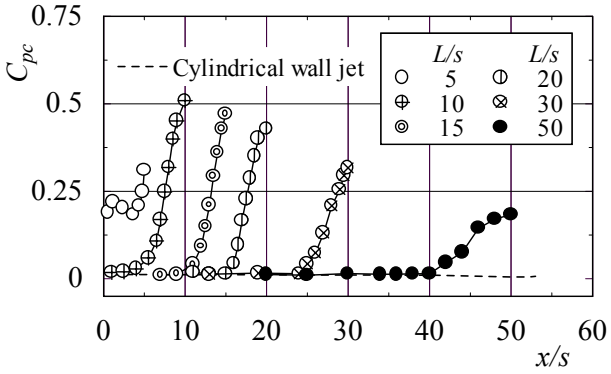

Fig.6 Variations in wall pressure on cylindrical wall

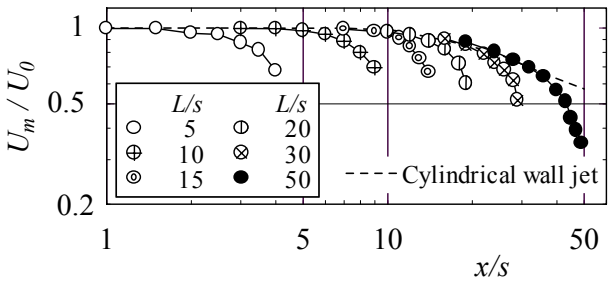

Fig. 7 Variations in maximum jet velocity

Comparing the mean velocity profile at x/s = 8 with the dotted line, it can be said that the position of y/b corresponding to the maximum value of U (i.e., U/Um = 1) for the impinging jet is about twice as far from that of the cylindrical wall jet. Again, at the region of y/b > 0.5, the decay of U for the impinging jet is faster than that for the cylindrical wall jet. The turbulent intensity profile at section x/s = 8 is much high with respect to the solid line near the cylindrical wall. Large deviation among the profile of turbulent intensity and that of the cylindrical wall jet is found in the region of y/b < 0.5.

Figure 5 also represents the distributions of the Reynolds stress component, $\overline{uv}$, at different sections. Comparing the Reynolds stress component, $\overline{uv}$, at section x/s = 8 with the dotted line, much large deviation is found in the region of y/b < 0.5 where the velocity gradient of the mean velocity is large.

Thus, the influence of the impingement is exerted on these profiles near the cylindrical wall in the region near the impingement plate.

Flow Properties In Region Before Impingement

The flow properties in the region from the nozzle exit to the impingement plate are shown in Figs. 6 to 9 for various nozzle-impingement distances, L/s = 5 to 50. In these figures the dotted lines represent the corresponding profiles of the cylindrical wall jet.

Figures 6 and 7 illustrate the variations in the wall static pressure on the cylindrical wall Cpc and the maximum jet velocity Um/Uo in the x-direction for various L/s, respectively. At a small value of L/s (L/s < 5), Cpc increases and Um/Uo decreases rapidly near the nozzle exit region. The flow is influenced by the impingement plate immediately out of the nozzle exit. However, when L/s is relatively large (L/s > 20), Cpc and Um/Uo vary gradually along the dotted line (cylindrical wall jet region), and departs from the dotted line near the impingement plate due to the impingement effect. Then Cpc increases suddenly and attains a maximum value on the impingement plate (This value is a stagnation pressure defined in Fig.10 later), whereas Um/Uo decreases rapidly in this region (impingement region). The position where Cpc departs from the dotted line as shown in Fig. 6 is in fairly agreement with that where Um/Uo decreases rapidly as shown in Fig.7. This position is defined by the beginning of the impingement region.

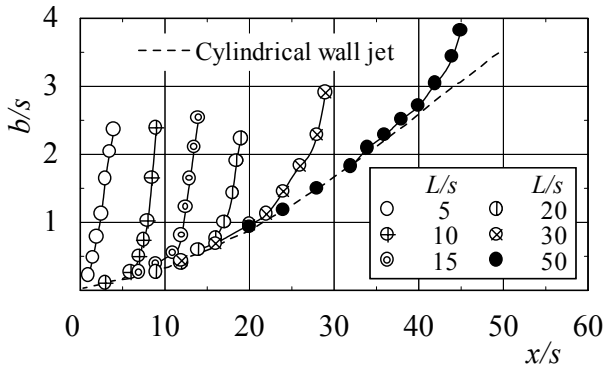

Fig.8 Variations in jet half-width

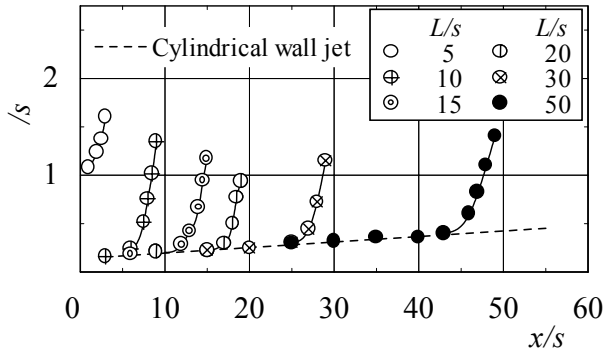

Fig.9 Variations in boundary layer thickness

Figures 8 and 9 represent the variations in the jet half-width b/s and the boundary layer thickness δ/s in the x-direction for various L/s, respectively. Here, the boundary layer thickness refers to the distance from the cylindrical wall to the point of maximum jet velocity. At a small value of L/s (L/s<5), both b/s and δ/s increase rapidly near the nozzle exit region due to the existence of the impingement plate immediately out of the nozzle exit. However, when L/s is relatively large (L/s > 20), b/s and δ/s vary gradually along the dotted line (cylindrical wall jet region), departing from it and then increase rapidly near the impingement plate (impingement region).

According to Figs. 6 to 9, it can be said that the flow field can be divided into two regions: a cylindrical wall jet region near the nozzle exit, in which the flow is hardly influenced at all by the impingement and an impingement region near the impingement plate where the flow is influenced by the impingement. The length of these regions is dependent on L/s.

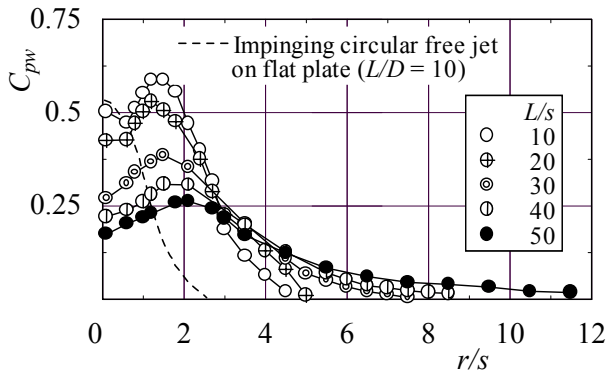

Fig.10 Variations in wall pressure on impingement plate along *r*-axis

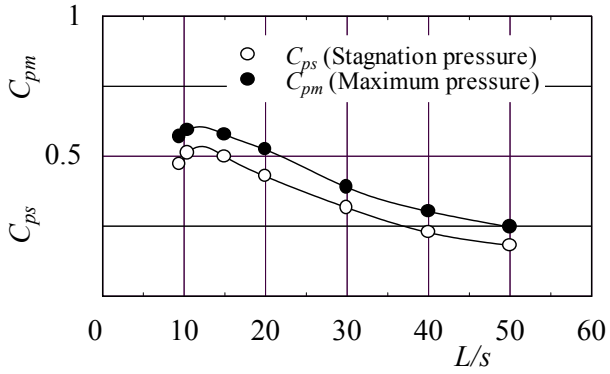

Fig.11 Relationship between maximum pressure and stagnation pressure on impingement plate and *L/s*

Flow Properties In Region After Impingement

Figure 10 shows the variations in the wall static pressure on the impingement plate *Cpw* along the *r*-axis for various *L/s*. Wall static pressure obtained by the impinging circular free jet on the flat plate at *L/D* = 10 is shown by the dotted line in the figure, in which *Cpw* decreases monotonously in the *r*-direction. Wall static pressures in the present experiment *Cpw* vary rather complicatedly with *L/s*. According to value of *L/s*, the *Cpw* profile has a minimum and a maximum value. The position where *Cpw* is maximum corresponds nearly to the reattachment point on the impingement plate[9]. Here, the pressure at the vicinity of the cylindrical wall surface (at $r/s \cong 0.05$) is named as the stagnation pressure.

The relationship between the maximum pressure *Cpm* and the stagnation pressure *Cps* on the impingement plate and *L/s* is shown in Fig. 11, values of which are obtained from Fig. 10. When *L/s* is relatively large (*L/s* >20), *Cpm* and *Cps* decrease gradually as *L/s* increases.

Figure 12 illustrates the velocity profiles in the sufficiently downstream region after impingement (r/s = 30) for various *L/s*. The solid line in this figure represents the velocity profile of the radial wall jet by Poreh et al.[10]. Here the velocity profiles are similar regardless of *L/s,* and are in good agreement with the solid line.

Figure 13 represents the variations in the maximum velocity of the radial wall jet *Vm/Uo* in the downstream direction after impingement

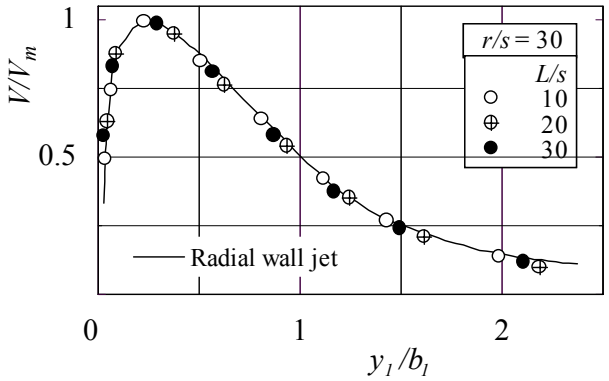

Fig.12 Velocity profile in sufficiently downstream region after impingement

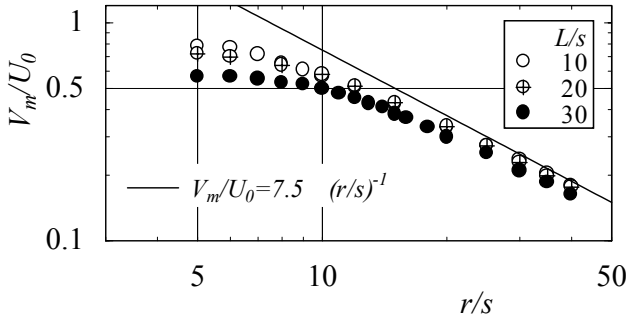

Fig.13 Variations in maximum velocity of radial wall jet

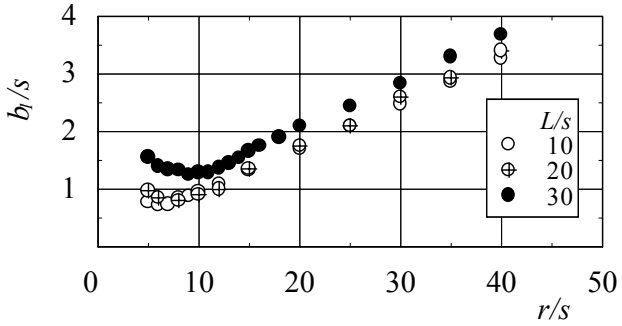

Fig.14 Variations in half-width of radial wall jet

for various *L/s*. The solid line in this figure represents the equation of a maximum velocity for a three-dimensional jet flow. According to this figure, *Vm/Uo* decreases slowly in the region of $5 < r/s < 10$, while it decreases rapidly in the more downstream region, and shows a good agreement with the solid line in the region of $r/s > 15$.

Figure 14 represents the variations in the half-width of the radial wall jet b_1/s in the downstream direction for various *L/s*. According to this figure, b_1/s decreases in the region of $5 < r/s < 10$, while it increases linearly in the region of $r/s > 15$.

From Figs. 12 to 14 it can be said that the radial wall jet region exists in a sufficiently downstream region after impingement where

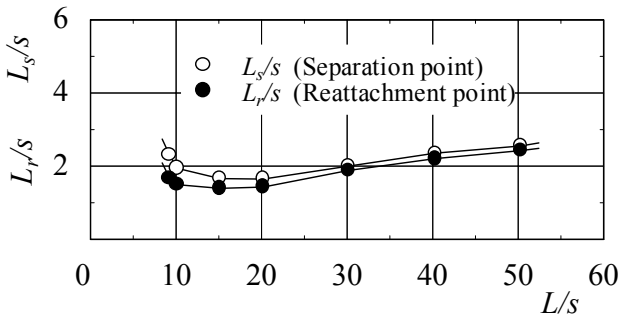

Fig.15 Relationship between positions of separation point and reattachment point and *L/s*

the jet flows radially along the impingement plate. This radial wall jet contains the three-dimensional characteristics.

Flow In Impingement Region

The relationship between the positions of the separation point on the cylindrical wall *Ls/s* and the reattachment point on the impingement plate *Lr/*s and *L/s* is shown in Fig.15. The separation point refers to the position where the velocity gradient at the cylindrical wall is zero in the velocity profile, and the reattachment point refers to the position where the wall static pressure on the impingement plate becomes maximum as shown in Fig.10.

When *L/s* is relatively large (*L/s* > 20), both *Ls/s* and *Lr/*s increase gradually as *L/s* increases. When *L/s* is quite small (*L/s* < 8), both values of *Ls/s* and *Lr/*s are not shown here. It was observed from the flow visualization by the tuft that the flow was unstable with a small disturbance and the directions of the flow near the separation point varied irregularly, so that the exact separation point could not be determined.

Figure 16 shows the mean flow vectors in the corner region between the cylindrical wall (*r/s* = 0) and the impingement plate (*x/s* = 30) for *L/s* = 30, in which the symbols △ and ▲ means the separation point on the cylindrical wall and the reattachment point on the impingement plate, respectively. The recirculating flow is formed in the corner region between the cylindrical wall and the impingement plate.

CONCLUSIONS

An experimental investigation into the effect of the nozzle-impingement distance *L/s* on the flow properties in different regions of the impinging cylindrical wall jet on the flat plate was carried out, and the following results were obtained:

(1) The flow field can be classified into three regions: a cylindrical wall jet region where the flow is almost unaffected by the impingement, an impingement region where the flow is influenced by the impingement, and a radial wall jet region where the jet flows radially along the impingement plate. The length of these regions is dependent on the nozzle-impingement distance *L/s*.

(2) When *L/s* is relatively large (*L/s* > 20), variations in the wall pressure *Cpc,* the maximum jet velocity *Um/Uo* , the jet half-width *b/s* and the boundary layer thickness δ*/s* agree with those of the cylindrical wall jet near the nozzle exit (cylindrical wall jet region), and diverge from them near the impingement plate due to the impingement effect (impingement region). The separation point on

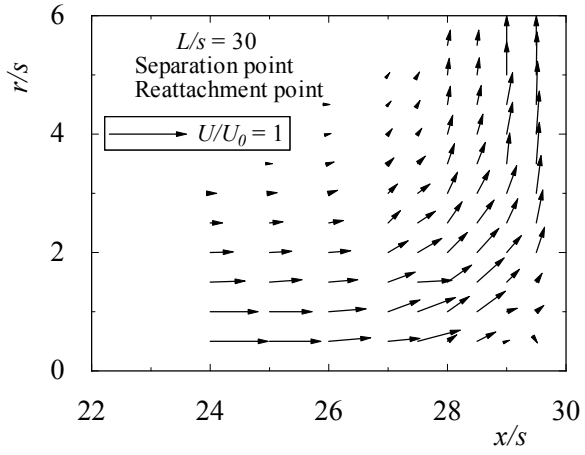

Fig.16 Mean flow vectors in corner region between cylindrical wall and impingement plate

the cylindrical wall *Ls/s* and the reattachment point on the impingement plate *Lr/*s increase gradually as *L/s* increases.

(3) When *L/s* is much small (*L/s* < 7), the cylindrical wall jet region does not exist. The flow is influenced by the impingement immediately out of the nozzle exit. The values of *Ls/s* and *Lr/*s cannot be determined because of the irregularity of the flow.

(4) In a sufficiently downstream region after impingement, the jet flows radially along the impingement plate (radial wall jet region), and contains the three-dimensional characteristics.

REFERENCES

(1) Abramovich, G. N., 1963, "The Theory of Turbulent Jets", The MIT Press, Massachusetts.

(2) Rajaratnam, N., 1976, "Turbulent Jets", Elsevier Scientific Publishing Company, Amsterdam.

(3) Schlichting, H., 1979, "Boundary Layer Theory", 7th ed., McGraw-Hill, New York.

(4) Bradshaw, P., and Love, E. M., 1961, "The Normal Impingement of a Circular Air Jet on a Flat Surface", Aeronaut. Res. Council, Lond., RM-No. 3205, pp. 1-8.

(5) Tani, I., and Komatsu, Y., 1964, "Impingement of a Round Jet on a Flat Surface", Proc. 11th Congr. Appl. Mech., Munich, pp. 672-676.

(6) Beltaos, S., and Rajaratnam, N., 1974, "Impinging Circular Turbulent Jets", Proceedings of A. S. C. E., J. Hydraul. Div., 100, pp. 1313-1328.

(7) Star, J. B., and Sparrow, E. M., 1967, "Experiments on a Turbulent Cylindrical Wall Jet", J. Fluid Mech., Vol. 29, pp. 495-512.

(8) Miller, D. R., and Comings, E. W., 1957, "Static Pressure Distribution in the Free Turbulent Jet", J. Fluid Mech., Vol. 3, pp. 1-15.

(9) Sawyer, R. A., 1960, "The Flow Due to a Two-Dimensional Jet Issuing Parallel to a Flat Plate", J. Fluid Mech., Vol.9, pp. 543-561.

(10) Poreh, M., Tsuei, Y. G., and Cermak, J. E., 1967, "Investigation of a Turbulent Radial Wall Jet", ASME, J. Appl. Mech., Vol. 34, pp. 457-463.